AD_____

Award Number: W81XWH-10-1-0843

TITLE: In Vivo PET Imaging of Myelin Damage and Repair in the Spinal Cord

PRINCIPAL INVESTIGATOR: Robert H. Miller, Ph.D.

CONTRACTING ORGANIZATION: Case Western Reserve University
Cleveland, OH 44106-7026

REPORT DATE: October 2012

TYPE OF REPORT: Annual

PREPARED FOR: U.S. Army Medical Research and Materiel Command
Fort Detrick, Maryland 21702-5012

REPORT DOCUMENTATION PAGE

Form Approved
OMB No. 0704-0188

1. REPORT DATE	**2. REPORT TYPE**	**3. DATES COVERED**
October 2012	Annual	30 September 2011 – 29 September 2012

4. TITLE AND SUBTITLE

In Vivo PET Imaging of Myelin Damage and Repair in the Spinal Cord

5a. CONTRACT NUMBER

5b. GRANT NUMBER
W81XWH-10-1-0843

5c. PROGRAM ELEMENT NUMBER

6. AUTHOR(S)

Dr. Robert H. Miller

E-Mail: rhm3@case.edu

5d. PROJECT NUMBER

5e. TASK NUMBER

5f. WORK UNIT NUMBER

7. PERFORMING ORGANIZATION NAME(S) AND ADDRESS(ES)

Case Western Reserve University
Cleveland, OH 44106-7026

8. PERFORMING ORGANIZATION REPORT NUMBER

9. SPONSORING / MONITORING AGENCY NAME(S) AND ADDRESS(ES)
U.S. Army Medical Research and Materiel Command
Fort Detrick, Maryland 21702-5012

10. SPONSOR/MONITOR'S ACRONYM(S)

11. SPONSOR/MONITOR'S REPORT NUMBER(S)

12. DISTRIBUTION / AVAILABILITY STATEMENT
Approved for Public Release; Distribution Unlimited

13. SUPPLEMENTARY NOTES

14. ABSTRACT

During the first funding cycle, we have worked closely with Dr Wang to develop a series of animal models to assess the efficacy of the imaging compounds that he has developed to detect demyelination and remyelination in the intact brain and spinal cord. We have also begun to test the ability of the imaging probes to assay remyelination in response to potential therapeutic treatments. The key research accomplishments are highlighted below:

1. Design, synthesis and evaluation of coumarin-based molecular probes for imaging of myelination. (Wang et al, J. Med. Chem. 2011)
2. Longitudinal imaging of myelination using a near infra-red probe. (Wang et al, J. Neuroscience 2011)
3. Longitudinal [11C]CIC-PET Imaging in the spinal cord of a rat model of focal demyelination.

15. SUBJECT TERMS
Positron emission tomography, imaging, myelination, molecular probes, multiple sclerosis.

16. SECURITY CLASSIFICATION OF:			**17. LIMITATION OF ABSTRACT**	**18. NUMBER OF PAGES**	**19a. NAME OF RESPONSIBLE PERSON**
a. REPORT	**b. ABSTRACT**	**c. THIS PAGE**			USAMRMC
U	U	U	UU	37	**19b. TELEPHONE NUMBER** *(include area code)*

Table of Contents

Page

INTRODUCTION

One of the major challenges to developing new treatments for demyelinating diseases such as Multiple Sclerosis (MS) is generating unambiguous data that the treatment is working, and more importantly that it is working through identifiable mechanisms. The majority of the current treatments available to patients with MS are targeted toward suppressing the immune system and its attack on myelin, oligodendrocytes and axons of the brain and spinal cord. Loss of myelin results in the failure of efficient conduction of axonal impulses leading to various neurological disabilities and cognitive impairment. In the healthy CNS, demyelinated axons can be reinvested with new myelin sheaths through an effective regenerative process. The remyelination process is thought to involve the recruitment of oligodendrocyte precursor cells (OPCs) that are subsequently activated and distributed to the damaged axons. However, the remyelination process is often disrupted in MS. This leads to incomplete myelin repair, and subsequent irreversible axonal damage. Given the central role the loss of myelin is thought to play in the generation of functional deficits in MS, my laboratory has spent the last 15 years trying to identify new ways to promote myelin repair. The overarching concept is that perhaps the combination of the inhibition of immune attack and the promotion of myelin repair within the CNS will generate more effective therapeutic approaches. This notion leads to the question of how to identify "myelin repair" in a longitudinal study of MS patients. Currently, the only way to unambiguously show myelin repair is through histological analyses of autopsy or biopsy material. To begin to redefine the MS therapy landscape and to develop approaches that facilitate the quantification of remyelination in a living longitudinal manner, we have joined forces with Dr. Yanming Wang in this Synergistic Idea Award from the Department of Defense to develop novel imaging agents that allow quantification of myelin repair in the living adult CNS. Dr. Wang is the leader of this project and is a leader in radiochemistry. His laboratory has generated a range of probes that bind with high selectivity to different molecular entities in

the brain and spinal cord. His report, which is a companion to this report covers in detail the generation and characterization of those probes. The Miller laboratory has a long track record of research into understanding the biology of oligodendrocyte development, the establishment of different model systems of demyelinating disease and the development of new therapeutic approaches for MS. This report will focus primarily on the identification of new therapeutics, model utilization and the advances we have made in these areas since the last submission of a progress report. The work is currently on a no cost extension and additional studies are awaiting commencement until the approval of the newly revised animal protocol. In the last progress report we documented the studies on new imaging compounds in a number of different animals models and pathological settings. In the last year we have extended these studies to determine whether we can use imaging modalities to guide therapy identification and selection. These studies represent the focus of the second specific aim of our synergistic award.

Body

The overall goal of this award is to develop new imaging probes that can be used to monitor the levels of myelination and remyelination in the adult human CNS, and to utilize these imaging modalities to assess the effectiveness of new therapies for promoting myelin repair. These studies will allow us to identify the best candidate(s) that are uniquely suited for future clinical trials. *We hypothesize that myelin repair can be achieved by therapeutic agents that stimulate the endogenous promotion of remyelination by host OPCs. Further, we specifically hypothesize that the efficacy of remyelinating agents can be quantified in vivo at various levels of myelination such that the regional distribution and concentration of probes will be consistent with the level of myelin neuropathology present*. Our approach in the first aims has been to further develop myelin-imaging agents that can longitudinal monitor myelin changes in different animal models of demyelination. In subsequent studies used PET imaging to evaluate the *in vivo* myelin repair properties of recently identified therapeutic agents. We then validate the *in vivo* studies by correlation with postmortem histology studies. Completion of this project will allow us to identify the lead candidate for Phase I clinical trial that can be initiated following completion of this project.

In the first year of this project, we reached the milestones outlined in Specific Aim 1. In the second year, we report our progress on the tasks listed in Specific Aim 2, which were centered around linking the imaging probes to therapeutic efficacy.

MATERIAL AND METHODS

Animal surgery and care was performed in accordance with the Institutional Animal Care and Use Committee of Case Western Reserve University.

Induction of focal demyelination in the spinal cord

A model of choice for the analyses of therapies that promote myelin repair in the adult CNS is the focal demyelination lesion model that develops as a result of the localized injection of a gliotoxin such as LPC into defined regions of the brain and spinal cord. This model has a number of advantages for characterization of imaging modalities and assessment of the efficacy of therapy treatment in myelin repair. For example, the lesion is accurately defined in time and space, the rate of endogenous repair is well established and the histological assessment of remyelination is unambiguous. In this model, LPC was directly injected into the spinal cord of Sprague-Dawley (SD) female rats (8-10 weeks old, 220-240 g) as previously described (Kerstetter et al., 2009). Animals were anesthetized using a mixture of rodent cocktail. For post-operative pain relief, Torbugesic (2 mg/kg) was subcutaneously administered prior to surgical procedure. A T10 laminectomy was performed by first making lateral longitudinal incisions in the paraspinal muscles from the middle of T-11 through the middle of T-12. A beveled microcapillary glass needle attached through small diameter tubing to a microinjection system (using a 10 µl Hamilton syringe) was then directed 1 mm into the dorsal column of the spinal cord with the aid of a Stoelting stereotaxic manipulator. LPC was injected into the dorsal column in a dose of 1.5 µl at 1% concentration, at a rate 0.25 µl/min. The needle was left in place for up to 5min before removal to ensure there was no backflow of the solution. The animals were allowed to recover in a clean cage on a heating pad and treated with analgesics as needed.

Induction of EAE in Lewis rats

Two sets of 8-week old female rats, 3 Lewis Rats and 3 Sprague Dawley rats were purchased from Charles River Laboratories, in Wilmington MA and maintained in the animal resource

center for one week after arrival. Animals were immunized with a emulsion of recombinant Myelin Oligodendrocyte Glycoprotein (rMOG 1-125, from Biogen Idec.), freshly prepared by initially diluting rMOG in 0.01M phosphate buffered saline (PBS, pH 7.4) to a final concentration of 2 mg/ml. Equal volumes of MOG/PBS and Complete Freund's Adjuvant were mixed thoroughly (CFA (2mg/ml), Chondrex, Inc, WA), the emulsion gently centrifuged, and loaded slowly into a 1-ml syringe for subcutaneous injection. Rats were anesthetized with rodent cocktail before emulsion injections, and administered 100 µl of inoculum by intradermal injection at the base of the tail. Each rat received 50 µg of rMOG 1-125. Animals were assessed for progression of disease after immunization, weighed and scored daily for signs of EAE according to the following scale: 0, no disease; 1, tail paralysis; 2, hind limb weakness; 3, hind limb paralysis; 4, hind limb paralysis and forelimb weakness; 5, moribund or dead.

Induction of neuroinflammation through delivery of lipopolysaccharide (LPS)

To determine whether the imaging approaches could distinguish between demyelination and inflammation in the CNS, a model of CNS inflammation was developed. Female SD rats (n=3, 6-8 weeks of age) were anesthetized with rodent cocktail and positioned in a stereotaxic frame (Stoelting). The scalp was incised and retracted so the cortex and corpus callosum could be targeted using the following stereotaxic coordinates: (relative to bregma) anterior–posterior (AP), 3.0 mm; medial–lateral (ML), 1.0mm; and dorsal–ventral (DV), 2.0 mm for cortex, and AP, 0.0 mm; ML, 2.0mm; and DV, 4.5 mm for corpus callosum. Two small holes were drilled in the skull, and a 33S gauge needle attached to a 10 µL Hamilton Syringe was lowered into the cortex and corpus callosum guided by the above coordinates. A mini injector pump (Stoelting) controlled the infusion of 3 µL of LPS (E.coli, serotype 055:B5, 1mg/ml) at a rate of 0.25 µL/min, after which the needle was left in place for 2 min to prevent liquid reflux out of the brain

parenchyma. The incision was then closed, and the animals were allowed to recover on a heating pad.

Histopathology

To validate the microPet studies, the same animals were subsequently sacrificed and used for histopathological analysis. The animals were sacrificed by a transcardial perfusion of saline followed by 4% polyformaldhyde (PFA) under terminal anesthesia. The spinal cord and brain were carefully removed and postfixed in 4% PFA overnight, followed by infusion with 10%, 20% and 30% sucrose solutions. Selected areas were sectioned at 20μm on a cryostat, and mounted directly onto Superfrost Plus microscope slides. The slides were then subject to either staining to detect neuroinflammation or Black Gold, Luxol Fast Blueor MeDa staining to detect myelin as previously described (Mi et al., 2007; Wu et al., 2008; Wang et al., 2009).

Detection of Neuroinflammation

Following cryoprotection in graded sucrose and rapid freezing, 20uM serial sections through regions of interest were prepared on a Microm HM525 cryostat. The sections were air-dried and kept at -20^{o}C until labeling. To detect neuroinflammation selected sections were brought to room temperature allowed to air-dry and rehydrated in PBS. The PBS was removed, and the sections blocked with 5-10% Normal Goat Serum in 0.1% Triton-X 100 in PBS for one hour at room temperature to reduce non-specific staining. The antibodies, IBA1 (Rabbit polyclonal, Wako Cat. #019-19741) or GFAP (Rabbit polyclonal, Dako Z0334), were diluted 1:500 in blocking medium containing 5% NGS, and the sections incubated overnight at 4^{o}C. The following day, the sections were rinsed, incubated 1.5 hours in the secondary antibody (Invitrogen goat anti-Rabbit IgG Alexa-594), washed thoroughly and mounted in Vectashield.

Sections were imaged on a Leica DM 5500B microscope and the images recorded using a Leica DFC 500 camera.

Ex vivo fluorescent tissue staining of myelin

To detect the labeling of myelin specific probes in sections of the CNS a dose of (25 mg/kg) of MeDAS was administered via tail-vein injection to a Female SD rat. At 2 hours post-injection, the rat was deeply anesthetized and perfused transcardially with saline and 4% paraformaldehyde (PFA) as described above. The brain and spinal cord were removed and postfixed by immersion in 4% PFA overnight, infused with 30% sucrose and embedded in the mounting compound OCT (Fisher Scientific, Suwanee, GA). Samples were sectioned at 20 μm on a microtome, and sections mounted on superfrost slides (Fisher Scientific) with fluoromount-G mounting media (Vector Laboratories, Burlingame, CA). Due to the fact that MeDAS is inherently fluorescent, the binding to white matter regions rich in myelin was directly detectable using a Leica DRMB microscope equipped for fluorescence.

HFG treatment

One major goal of this program is to determine whether one can use longitudinal imaging to assess the efficacy of therapeutic approaches to myelin repair. The selected therapy for these studies was hepatocyte growth factor (HGF), which we recently demonstrated was one of the primary components of mesenchymal stem cell conditioned medium responsible for myelin repair (Bai et al 2012). In these studies an LPC lesion was induced as described above, and the animals were treated with 2 doses of HGF systemically. Because there is an initial immunological response to the demyelinating lesion, delivery of the first dose was delayed for 4 days after lesion induction. Animals were randomly assigned to either control (saline, n=6) or

experimental (HGF treatment, n=8) groups. The experimental group received 0.4 and 0.8μg/Kg of HGF via tail vein injection on days 4, 6, and 12 post lesion. The controls received an equivalent volume of saline, and the animals were imaged on days 7, 14, and 21 post LPC treatment. At the termination of the study the animals were sacrificed and the level of myelin repair in the lesion compared between control and experimental animals.

MicroPET/CT imaging of spinal cord and data acquisition

PET imaging of [^{11}C]MeDAS was performed using a Siemens Inveon microPET/CT scanner in the Case Center for Imaging Research. For better anatomic localization, CT co-registration was applied. For LPC treated rats, PET/CT scans were performed on days 0, 7, 14, and 21, following LPC injections in spinal cord. For EAE rats, PET scans were performed on day 0, and the first, second, and third disease episodes after MOG induction. The rats were fasted overnight prior to imaging, but had access to water. Their diet was replenished after imaging. Before PET imaging, CT scout view was taken to ensure most of the vertebrae, especially the ilium, were placed in the co-scan field of view (FOV) where the highest image resolution and sensitivity is achieved. Approximately 37 MBq of [^{11}C]MeDAS was injected through the tail vein, and dynamic microPET data acquisition was performed in a list mode immediately. During the scans, body temperature of the anesthetized rats was maintained at 34+/-2°C with a heating lamp. Once the dynamic acquisition was done, a CT acquisition scan was performed for attenuation correction.

Quantitative image analysis

Quantitative image analysis of the uptake of [^{11}C]MeDAS in spinal cord was performed using Carimas II software. This program allows an ROI to be extrapolated from the reconstructed microPET image frames in order to determine the SUV in a specific region. Based on the PET

and CT co-registered images, the rat's ilium was used as a marker to accurately identify vertebrae. For LPC treated rats, lesion vertebrae (Thoracic 11 and Thoracic12) were then defined as the regions of interest (ROI). For EAE rats, every single rat vertebrae (from Thoracic 8 to Lumbar 1) was defined as a ROI. The radioactivity data were decay-corrected and normalized by the body weight of the rats, and amount of [^{11}C]MeDAS injected. Radioactivity concentration in the spinal cord is expressed in terms of standard uptake value (SUV) [(μCi/cc)/(uCi/g)] as a function of time. The time activity curve (TAC) for each vertebra was obtained.

MicroPET imaging in acute neuroinflammation rat model and data acquisition

Following the induction of CNS inflammation, rats were placed in an Inveon microPET scanner under anesthesia. After a 10 min transmission scan with a Co-57 source, 37 MBq of [^{11}C]MeDAS was administered via tail vein injection, and immediately followed by a dynamic acquisition of up to 90 min. A two-dimensional OSEM algorithm was used for image reconstruction. Decay, attenuation, and scatter correction were all performed during the image histogram and reconstruction processes. For better anatomic localization, a MRI scan was also performed. After microPET imaging, the same bed was transferred to a MRI scanner (Bruker Biospin 7.0T, Billerica, MA). The rat's head was well positioned in the center of the rat coil. A rapid-acquisition relaxation-enhanced (RARE) analysis (TR/TE = 2000/40 ms, 4 echoes, FOV = 45 mm × 45 mm, matrix = 256 × 256) was used to acquire 15 contiguous 1 mm axial images of each animal's brain. Co-registration of MRI and PET images was conducted using the MATLAB-based program Compartmental Model Kinetic Analysis Tool (COMKAT). For quantitative image analysis, the whole brain was considered as a ROI, and was defined based on the co-registered images to measure the radioactivity concentration in the whole brain. The radioactivity data was decay corrected and normalized by the body weight of the rats, and

amount of [^{11}C]MeDAS injected.

Statistical analysis

In this study, all data is expressed as a mean±SD. A Student's t test was used to evaluate if there is any significant difference between each groups of studies. A *p* value of <0.05 was accepted as significant.

RESULTS

In vitro tissue staining of the spinal cord

MeDAS is a fluorescent compound with maximum excitation and emission wavelengths of 363 and 419 nm, respectively (Wu et al., 2008). So the myelin binding property of MeDAS can be evaluated based directly on fluorescent microscopy. In a first set of studies, section of rat spinal cord were directly incubated in a solution of MeDAS in 10% DMSO. For this purpose, a series of axial sections of the spinal cord were prepared so that both myelin-rich white matter and myelin-deficient gray matter could be visualized. To determine whether MeDAS could accurately identify changes in the normal pattern of myelination, the distribution of labeling i was compared in sections taken from wild type control animals as well as from animals that had previously received either an LPC demyelinating lesion or had ongoing EAE. To validate MeDAS staining the pattern of binding was correlated with that seen with Black-Gold staining, on adjacent sections. At a 10μM concentration, MeDAS selectively stained the spinal cord white matter and significantly lower levels of MeDas labeling were seen in the central gray matter of the spinal cord. This differential distribution is consistent with the pattern of labeling seen with black gold staining and reflects the differential levels of myelin in white and gray matter in the spinal cord (**Figures 1 A and 1B**).

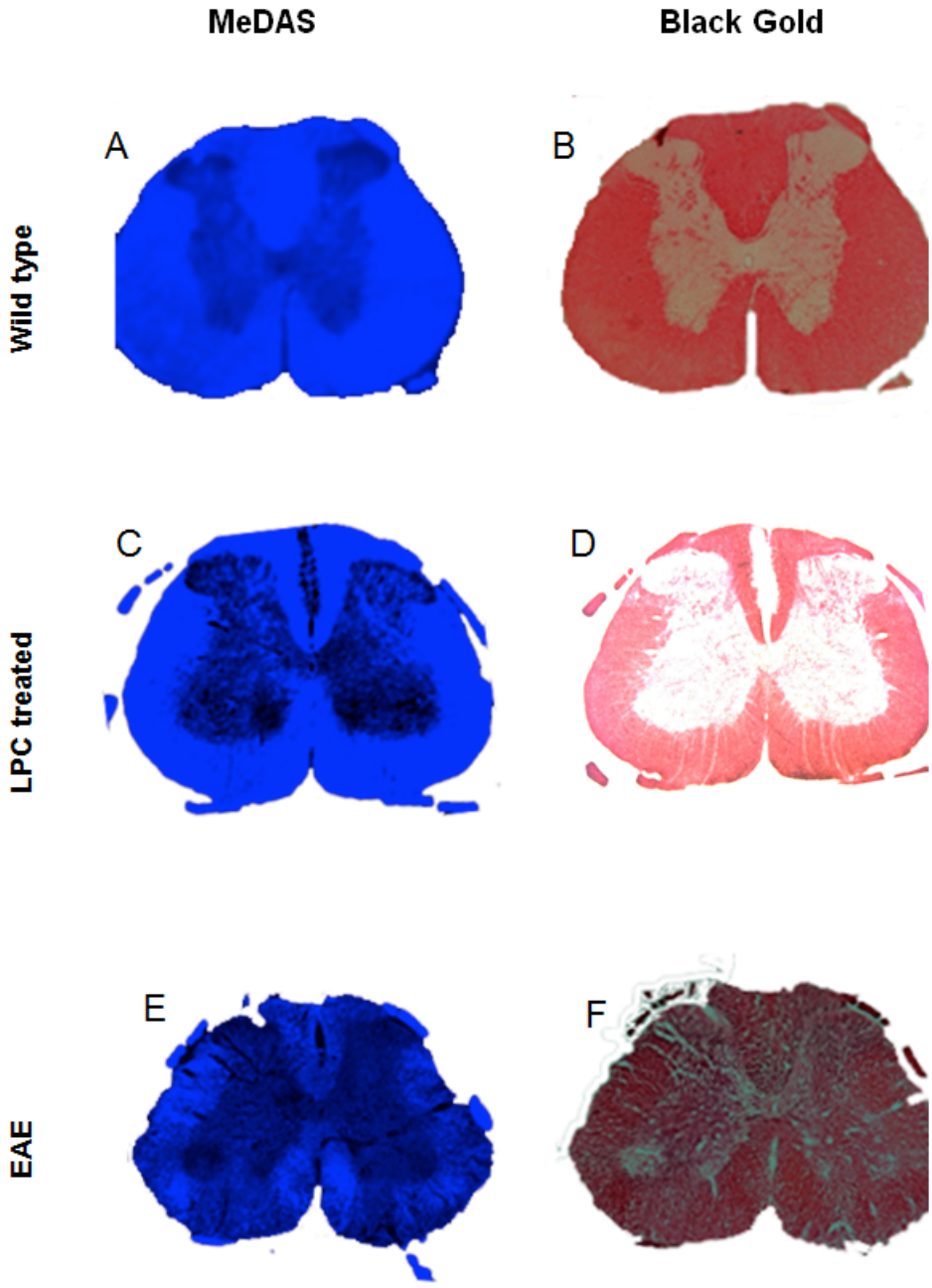

Figure 1. *In vitro* MeDAS staining of the spinal cord tissue sections from wild-type, LPC-treated and EAE rats that are consistent with Black-Gold staining in adjacent tissue sections.

The staining of MeDAS correlates directly with the presence of myelin sheaths. In the models of demyelination, the localized loss of myelin sheaths resulted in a significant disruption in the

binding of MeDAS. This was observed in fluorescent MeDAS staining of the spinal cord, with focal demyelination in the white matter that was induced by stereotactic injection of LPC. Our previous studies have shown that LPC treatment led to focal myelin loss with significant sparing of other cell types, such as axons and astrocytes (Wang et al., 2009). As shown in **Figure 1C and 1D**, the demyelinated foci in the dorsal columns of the spinal cord are readily visualized by MeDAS fluorescence, and provide a image that was identical to Black-Gold staining on adjacent sections. Thus, MeDAS is capable of detecting demyelinated lesions. Similarly, in the spinal cord of EAE rats where the regions of demyelination are less reproducible but often located at the periphery of the spinal cord, MeDAS staining showed profound demyelination across the peripheral white matter in parts of the most affected vertebrae, as confirmed by the Black-Gold staining (**Figure 1E and 1F**). These data provide strong support of the notion that MeDAS is selectively binding to myelin sheaths and that the level of binding can distinguish areas of myelin perturbation.

***In situ* detection of myelin in rat brain and the spinal cord**

Following *in vitro* tissue staining, we investigated the ability of MeDAS to stain myelin tracts *in situ*. In these studies a single dose of MeDAS (20 mg/kg) was administered to wild-type SD rats via tail vein injection. Two hours later, upon perfusion, the brain and the spinal cord were then removed and sectioned, and the fluorescent MeDAS distribution was directly examined under fluorescent microscopy. As shown in **Figure 2**, the myelinated corpus callosum and the white matter of spinal cord are clearly visualized by MeDAS staining with fluorescent patterns that were consistent with Black-Gold staining in adjacent sections. These studies suggested that MeDAS readily entered the brain and spinal cord and selectively labeled the respective myelinated regions in the white matter.

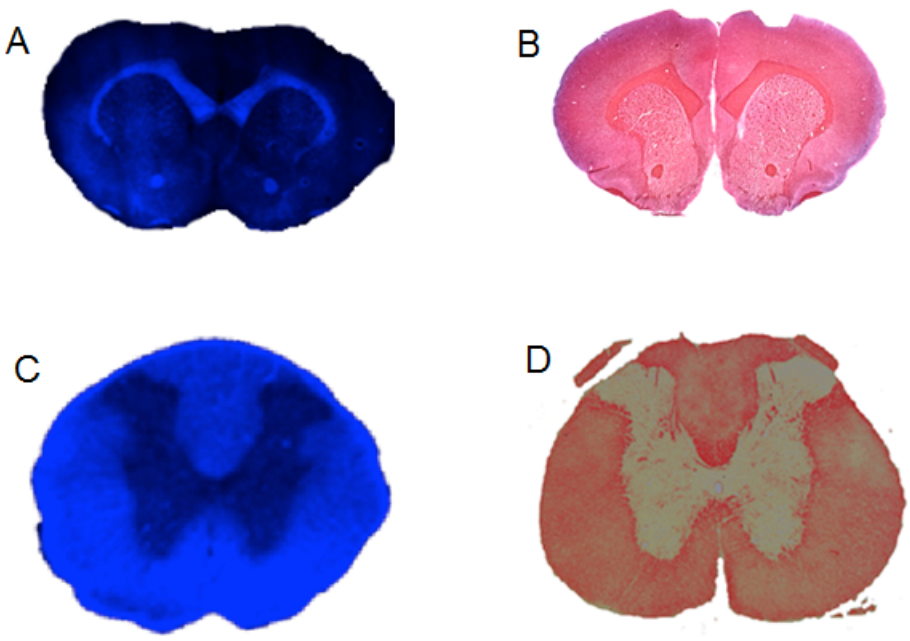

Figure 2. *In situ* MeDAS staining of myelin sheaths in the brain (A) and spinal cord (C) two hours after single dose (20 mg/kg) administration via tail vein injection, which correlates with Black-Gold staining in adjacent tissue sections (B and D, respectively).

These studies provided confidence that the imaging probe had the characteristics suitable to allow the longitudinal analyses of myelin repair in animal models of MS. The Wang group 9 then undertook a series of studies to examine biodistribution and in vivo competition studies using earlier developed probes (Wang et al., 2010). These data are outlined in detail in his report, but briefly showed that MeDAS rapidly passed through the blood-brain barrier and its retention was higher in neural tissue than any other tissue, although some residual binding was seen in bone and adrenals. In a series of competitive binding studies using a previously developed myelin-binding agent (BMB), as a blocking agent, which has shown high affinity for myelin (Stankoff et al., 2006) they showed that when the rats were pretreated with BMB (10 mg/kg) at 3 hrs prior to [^{11}C]MeDAS-PET imaging, the specific binding was significantly reduced. At 40 min post-injection, for example, the specific binding to myelin rich areas in

pretreated compared to control rats was reduced by approximately 50% in all the regions.

Effects of neuroinflammation on PET imaging of demyelination

One challenge to developing an imaging probe for a demyelinating disease such as MS is that it has to be able to distinguish between frank demyelination and neuroinflammation. Frequently, both are present in MS lesions and while it is critical to regulate CNS inflammation understanding the targets of pharmacological or cellular therapies require that the imaging probe is capable of distinguishing between the two pathologies. To determine if neuroinflammation has any effects on [^{11}C]MeDAS uptake, we prepared an acute neuroinflammation model by stereotaxic injection of LPS to the rat brain (Wenk et al., 2004). Subsequent histological analysis showed that one day after injection, profound inflammation developed in the rat brain while myelin sheaths remained intact. Neuroinflammation is characterized by increased activation of microglial cells, the macrophage equivalent in the brain and spinal cord as well as an activation of astrocytes. Microglial cells can be identified through the expression of IBA1 and antibodies to IBA1 selectively bind to microglia. The reaction of astrocytes to neuroinflammation is complex and results in both hypertrophy and occasionally proliferation. One characteristic change of reactive astrocytes is significant upregulation of the expression of the intermediate filament protein glial fibrillary acid protein (GFAP). Following LPS injection immunohistology showed profound microglia activation and macrophages in the brain by IBA1 staining (**Figure 3A** and **3E**). Reactive astrocytes were also detected by GFAP staining (**Figure 3B** and **3F**). In the meantime, the myelin integrity remained intact as demonstrated by Luxol Fast Blue staining (**Figure 4C** and **4G**), and *in vitro* MeDAS staining (**Figure 3D** and **3H**). Using this neuroinflammation rat model, we conducted PET studies to determine [^{11}C]MeDAS uptake before and after the inflammation was induced and to assess the effects of inflammation on that uptake. As shown in **Figure 3I** and **3J**,

[^{11}C]MeDAS uptake was practically identical before and after LPS treatment. Thus, induction of inflammation did not alter the pharmacokinetics of [^{11}C]MeDAS in the brain.

These studies suggested that [^{11}C]MeDAS-PET is a specific imaging marker of demyelination, and that this is not significantly altered by coincident neuroinflammation.

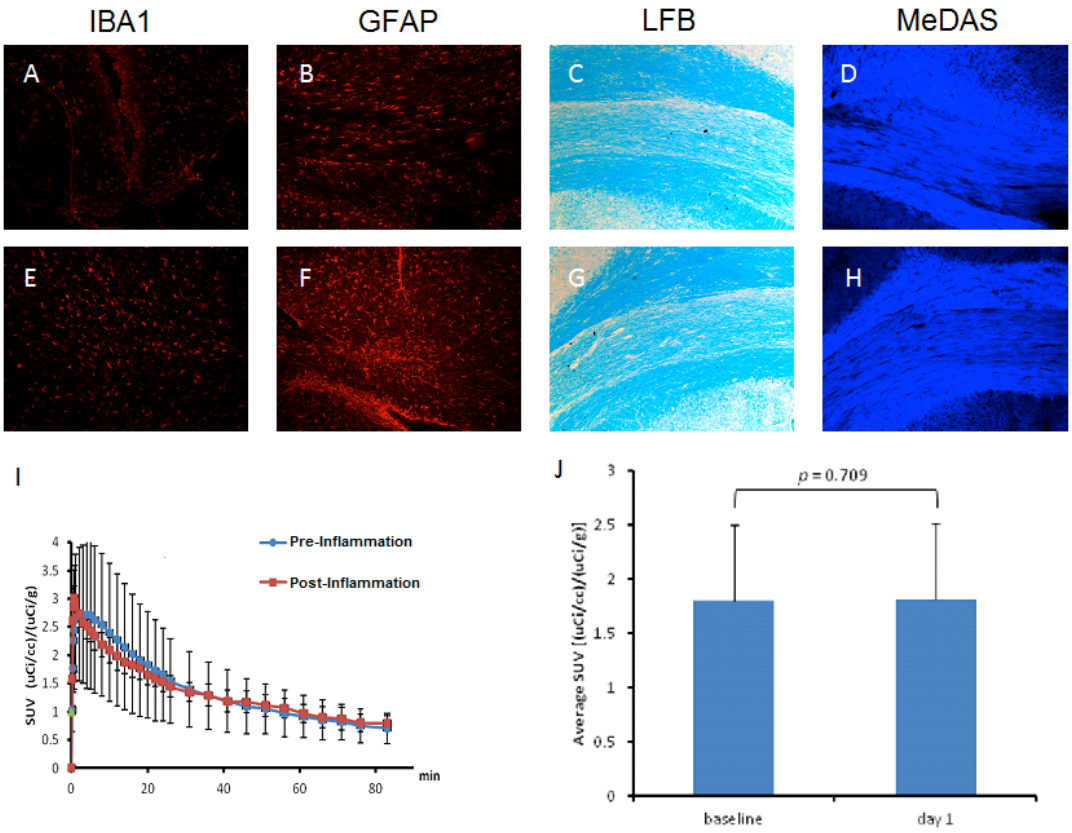

Figure 3: Immunohistochemical staining and [^{11}C]MeDAS-PET studies in the rat brain at 24 hours after induction of neuroinflammation by LPS. A-D: Immunohistochemical staining of the right hemisphere of the rat brain including IBA1 staining of activated microglia and macrophages (A), GFAP staining of astrocytes in reactive form (B), Luxol Fast Blue and MeDAS staining of intact myelin tract (C and D). E-H: the corresponding staining results in the left hemisphere. I. [^{11}C]MeDAS uptake as a function of time over the 90 min scan showing similar pharmacokinetic profiles before and after induction

of inflammation. J. Average brain uptake of [^{11}C]MeDAS over the 90 min of PET scan suggesting that neuroinflammation has no effects on [^{11}C]MeDAS uptake.

Longitudinal PET imaging of the spinal cord in a LPC rat model

We then evaluated the ability of [^{11}C]MeDAS-PET to longitudinally assess myelin content in the spinal cord *in vivo*. To quantitatively characterize demyelination and remyelination, we first induced a focal demyelinated lesion (T11-12) by stereotactic injection of LPC to the spinal cord. The rat was then subjected to a serial PET/CT imaging at the peak of demyelination (7 days post injection), and during the course of remyelination (14 and 21 days post injection). As shown in **Figure 4A**, the rat spinal cord was readily visualized by [^{11}C]MeDAS-PET with high specificity and sensitivity. The uptake of [^{11}C]MeDAS in the affected region of the spinal cord at various time points was quantified. As shown in **Figure 5B**, [^{11}C]MeDAS uptake was lowest at day 7 when demyelination was peaked. At day 14 and day 21 post injection, [^{11}C]MeDAS uptake gradually increased due to the process of remyelination.

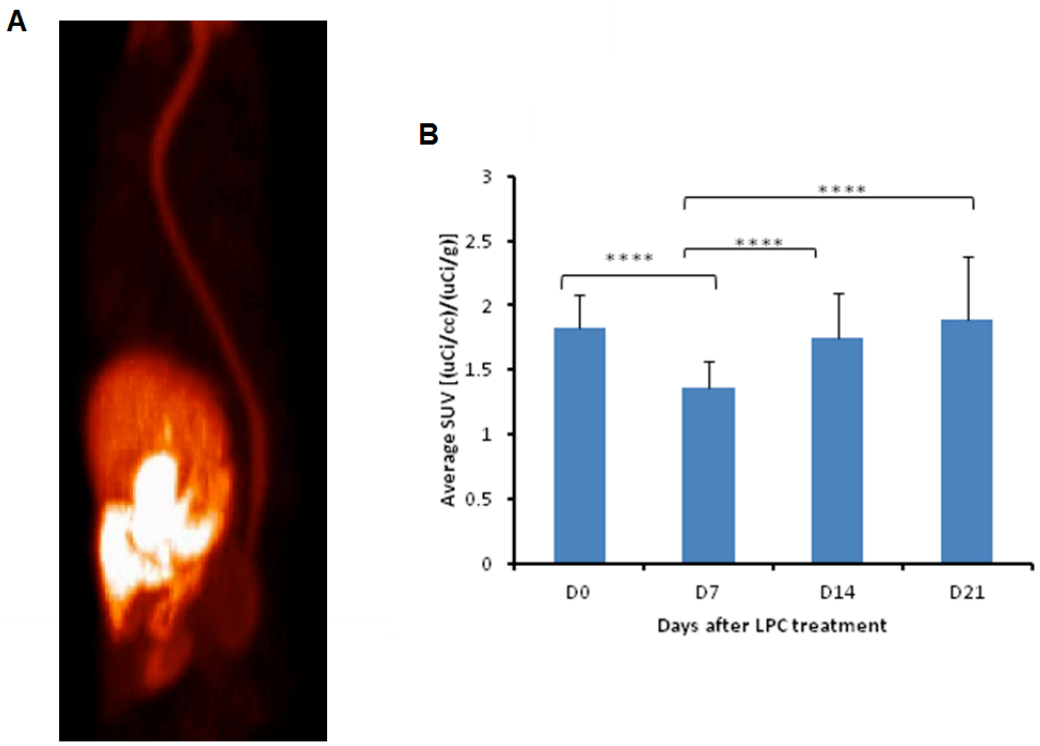

Figure 4. A: representitative PET image of the rat spinal cord. B: Longitudinal PET studies in the LPC-treated rats over 21 days. The average uptake in the spinal cord (T11-12) was quantified on day 0, 7, 14, and 21. On day 7 of demyelination, the uptake of [^{11}C]MeDAS in the T11-T12 region decreased by 34% compared to day 0. On day 14 and 21 of remyelination, the uptake of [^{11}C]MeDAS in the T11-T12 region increased by 22% and 28%, respectively, compared to day 7.

The level of remyelinaiton was confirmed using toludine blue labeled epon sections and representative samples are shown in **Figure 5**.

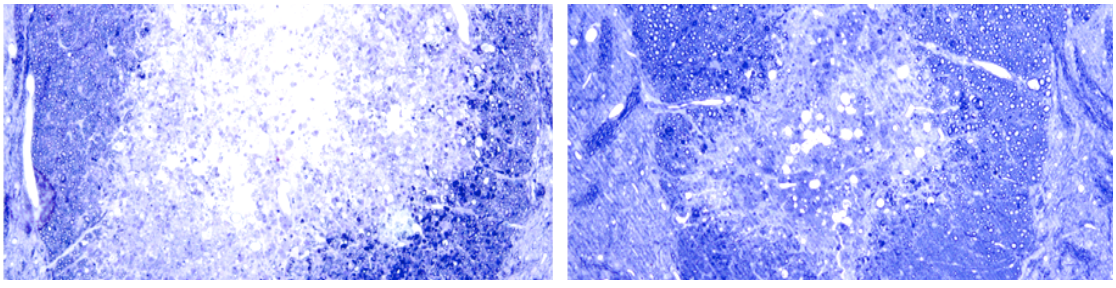

I week post LPC

3 weeks post LPC

Figure 5 At one week post PLC lesions the lesion area is significantly reduced in the level of myelin and the number of myelinated axons as shown by the relatively light level of toluidine blue staining. By contrast, at 3 weeks post LPC while the level of myelination as not returned to pre-lesion levels it is significantly higher than at earlier post lesion times.

Longitudinal PET imaging of the spinal cord in EAE rat model

While the LPC model represents pure demyelination/remyelination, EAE is an animal model that closely mimics the MS pathology because it incorporates immunological induction of neuropathology. We therefeore conducted a series of [^{11}C]MeDAS-PET imaging in an EAE rat model to longitudinally monitor myelination in the spinal cord. In this study, EAE was induced by immunizing 3 SD rats and 3 Lewis rats with MOG1-125 peptide. Starting at day 7 after immunization, the SD and Lewis rats developed paralysis of hind limbs, with an EAE score reaching 3.0 or above in a relapsing and remitting pattern. In this study longitudinal PET imaging was conducted at three time remitting points of the disease and [^{11}C]MeDAS uptake in different vertebrae regions was quantified. In the EAE SD rats, [^{11}C]MeDAS was not evenly distributed across the spinal cord. Before immunization, [^{11}C]MeDAS uptake was relatively high in part of the thoracic region (T10-T13) (**Figure 6A**). After immunization, [^{11}C]MeDAS uptake was significantly decreased across the whole spinal cord, particularly between thoracic regions T10-T13 (**Figure 6B**). The average [^{11}C]MeDAS uptake was determined from L3 to T8 at the three episodes on days 15, 25, and 42 (**Figure 6C**). Compared to pre-immunization, the average [^{11}C]MeDAS uptake decreased significantly at all three episodes (**Figure 6C**). Particularly at the third episode on day 42 when the EAE score was almost 5.0, [^{11}C]MeDAS uptake reached the lowest level (**Figure 6D**). The greatest change was observed in the region between T10-T13 as shown in the representative PET and CT fusion image of the spinal cord in the SD rat on day 42 after immunization with MOG1-125, which was reconstructed based on

uptake of [^{11}C]MeDAS (**Figure 7**). These data suggest that the pattern of demyelination is variable along the length of the spinal cord and that the level of pathology is variable over time. Such observations are entirely consistent with previous histological studies in this model.

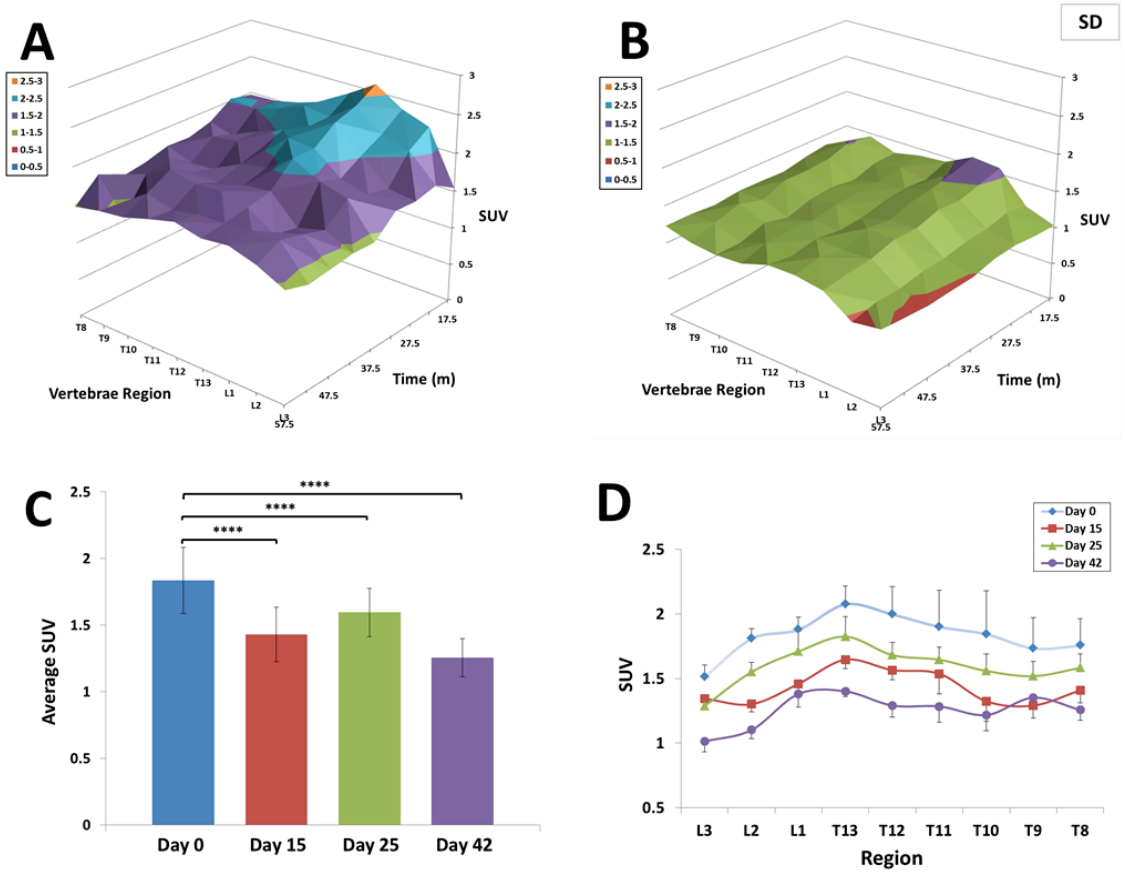

Figure 6. A: [^{11}C]MeDAS uptake across regions L3-T8 from 17.5 min to 57.5 min of a control SD rat. B: [^{11}C]MeDAS uptake across regions L3-T8 from 17.5 min to 57.5 min of an EAE SD rat after immunization with MOG1-125. Note homogenous demyelination in these regions, characterized by a lower SUV. C: Average SUV values over the L3-T8 region in the SD rat on day 0, 15, 25, and 42. D: Average SUV values by spinal region in SD rat for each scan. Note the most premilent changes occur in the L3-T8 region. Error bars refer to absolute error.

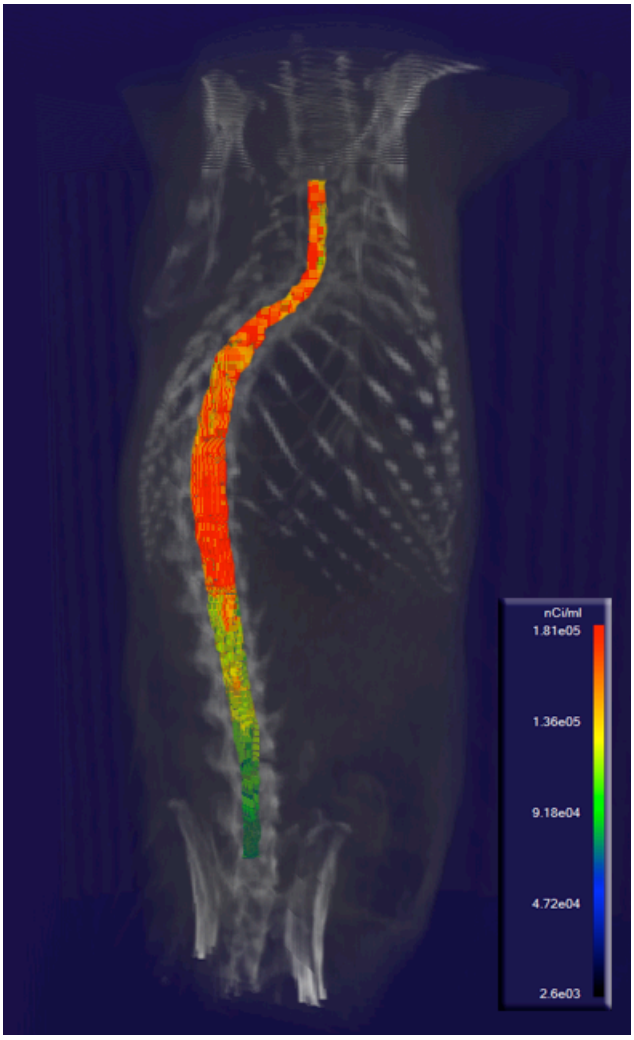

Figure 7. Three-dimentional PET and CT fusion image of the spinal cord in a SD rat on day 42 after immunization with MOG1-125.

In the EAE Lewis rats, similar pattern of [^{11}C]MeDAS distribution was observed. Before immunization, [^{11}C]MeDAS uptake was relatively high in the thoracic region between T9-T13 (**Figure 8A**). After immunization, [^{11}C]MeDAS uptake decreased significantly in the lumbar regions (L1-L6) compared to other regions in the spinal cord (**Figure 8B**). The average [^{11}C]MeDAS uptake was then determined at the three peaks of the disease: on days 26, 33,

and 39 (**Figure 8C**). This is particularly apparent at the third episode when the EAE symptom was most severe. Unlike the EAE SD rats, the EAE Lewis rats showed the most difference in the lumbar region between L1 and L6 (**Figure 8D**). Post-mortem histochemical staining using both MeDAS and Black-Gold displayed significantly low fluorescence in the white matter of the spinal cord (**Figure 2E and 2F).**

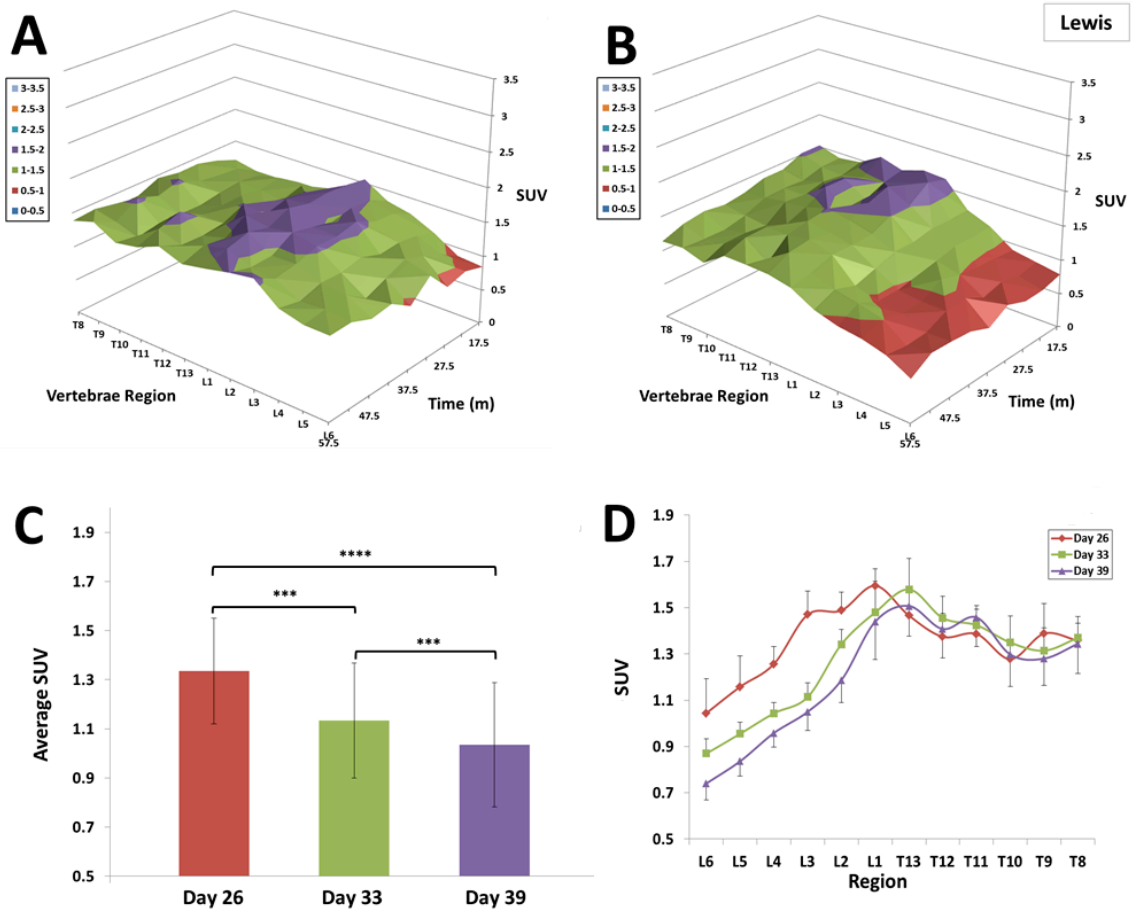

Figure 8. A: [^{11}C]MeDAS uptake across regions L6-T8 from 17.5 min to 57.5 min of a control Lewis rat. B: [^{11}C]MeDAS uptake across regions L6-T8 from 17.5m to 57.5m of an EAE Lewis rat. Note significant demyelination in the Lumbar vertebrae, characterized by a lower SUV in these areas. C:

Average SUV values over the L6-L1 region in the EAE Lewis rat on day 26, 33, and 39 after immunization of MOG1-125. D: Average SUV values in the L6-T8 region in the EAE Lewis rat for each

The Wang group then went on to characterize the detection limits of demyelination and remyelination and assess the different factors that contribute to the limits of detection of demyelination and remyelination (Wang et al., 2011).

Image-guided myelin repair therapy

In previous studies we have demonstrated that the functional recovery that is seen following treatment of demyelinated animals with mesenchymal stem cells is dependent on their release of hepatocyte growth factor (**Figure 9)** (Bai et al., 2012).

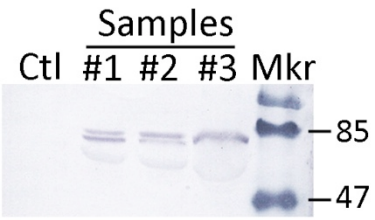

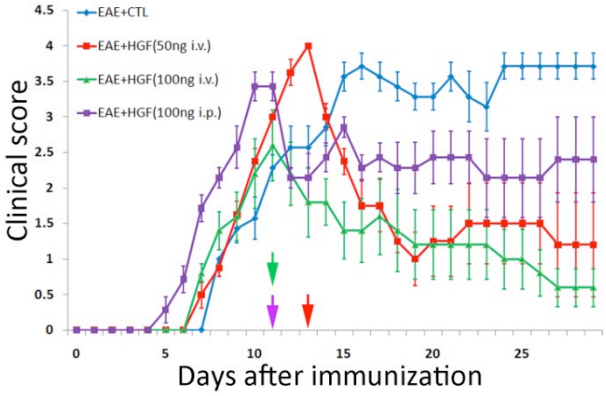

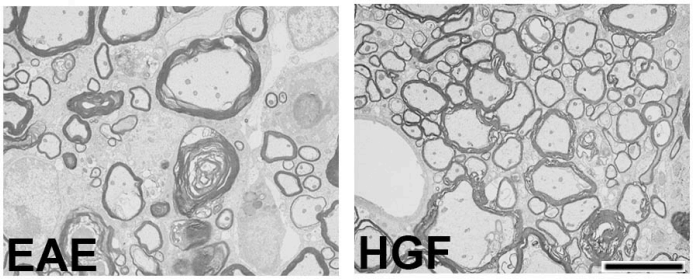

Figure 9. Hepatocyte growth factor is present in MSC conditioned medium and enhances functional recovery in EAE. Ultrastructural analysis demonstrates that HGF treated animals have significantly enhanced levels of remyelination compared to untreated controls.

Based on the longitudinal studies, we conducted the first image-guided myelin repair therapy in a rat model of focal demyelination to monitor myelin changes in the spinal cord and determine the dose response of HGF, a multifunctional growth factor that has been proven to be the effective component in MSC therapy of myelin repair (Figure 9, Bai et al., 2012). In this study,

rats were first treated with LPC to induce demyelination in the spinal cord. On days 7 and 9, the rats were sequentially treated with HGF, and imaged by [^{11}C]MeDAS-PET on days 7, 14, and 21. At a dose of 100 ng/rat or 0.4 μg/kg, the HGF-treated rats displayed an increased [^{11}C]MeDAS uptake in the spinal cord compared to the control rats. Quantitative analysis showed the HGF treatment caused the average uptake in the demyelinated regions to be 31% and 14% greater at day 14 and 21 respectively, when compared with day 7 (**Figure 10)**. When the rats were treated with a higher dose of HGF (i.e. 200 ng/rat or 0.8 ug/kg), the maximal remyelinating effect was observed to be 33% and 35% on days 14 and 21, respectively. Note there is only a significant difference in the amount of remyelination on day 21, on day 14 the difference in remyelination provided by the additional dose of HGF is not significant. The imaging results were confirmed by double-blinded immunohistochemical observations of postmortem tissue sections harvested at each time point (Bai et al., 2012).

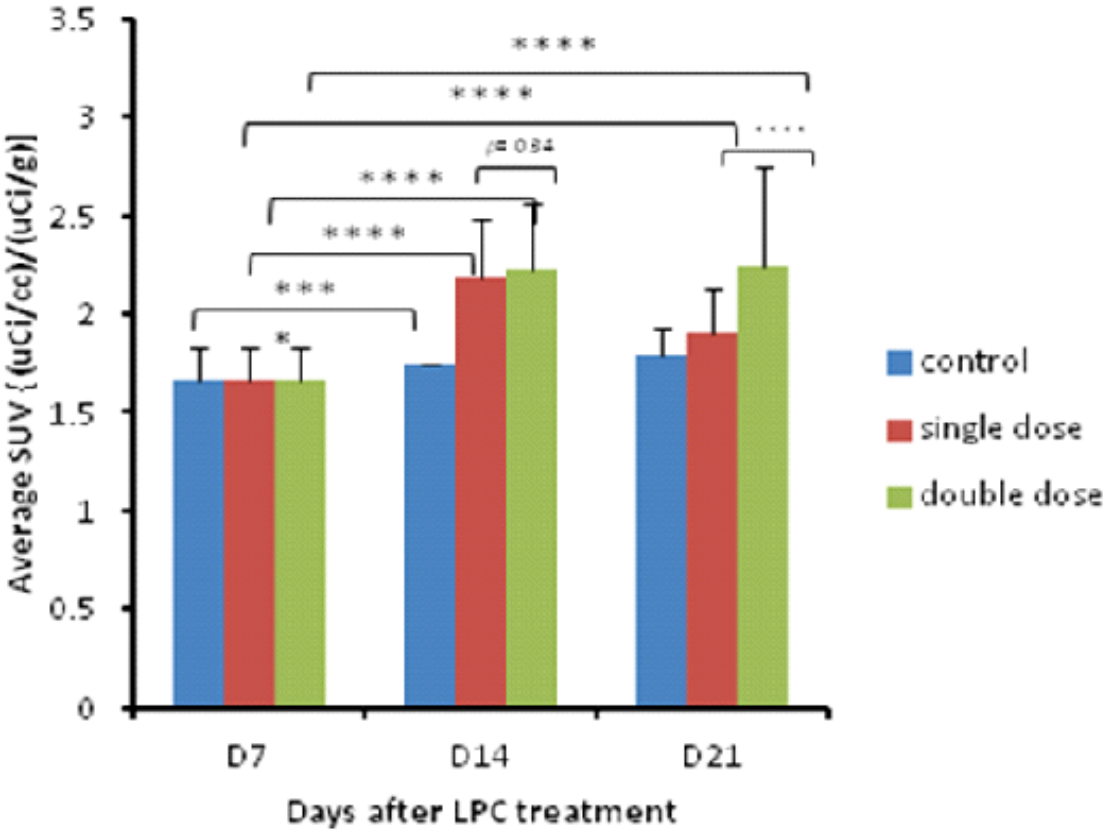

Figure 10. Longitudinal quantitative PET analysis of myelin changes in the spinal cord (T11-12) of a LPC-treated rat model on Day 7, 14, and 21 following HGF-treatment. Increased specific uptake of [^{11}C]MeDAS in spinal cords of HGF treated versus control. Following HGF treatment at a dose of 100 ng/rat or 0.4 ug/kg, the average uptake of [^{11}C]MeDAS increased by 31% and 14% compared to the control on day 14 and 21, respectively. When the HGF dose were doubled, the average uptake of [^{11}C]MeDAS increased by 33% and 35% compared to the control on day 14 and 21, respectively.

Rodent-based dosimetry estimates of [^{11}C]MeDAS

In order to conduct future characterization of [^{11}C]MeDAS in humans, rodent-based dosimetry of [^{11}C]MeDAS was estimated. The single organ and whole body radiation exposure associated with [^{11}C]MeDAS injection was determined from the biodistribution data obtained in mice. Based on the biodistribution, dosimetry was estimated using OLINDA/EXM(Stabin et al., 2005)

software. Based on an extrapolation of the animal data to humans, the radiation doses estimated for various human organs are summarized in **Table 2**.

Table 2. Organ and whole body extrapolated human dosimetry estimation.

Target Organ	mSv/MBq	rem/mCi
Adrenals	4.31E-03	1.59E-02
Brain	1.89E-03	7.01E-03
Breasts	2.25E-03	8.34E-03
Gallbladder Wall	3.28E-03	1.21E-02
LLI Wall	3.03E-03	1.12E-02
Small Intestine	3.10E-03	1.15E-02
Stomach Wall	2.93E-03	1.08E-02
ULI Wall	3.06E-03	1.13E-02
Heart Wall	2.30E-03	8.49E-03
Kidneys	2.72E-03	1.00E-02
Liver	4.64E-03	1.72E-02
Lungs	2.91E-03	1.08E-02
Muscle	2.60E-03	9.61E-03
Ovaries	3.12E-03	1.15E-02
Pancreas	3.15E-03	1.16E-02
Red Marrow	3.62E-03	1.34E-02
Osteogenic Cells	6.76E-03	2.50E-02
Skin	2.14E-03	7.92E-03
Spleen	2.41E-03	8.94E-03
Testes	2.58E-03	9.53E-03
Thymus	2.69E-03	9.94E-03
Thyroid	2.69E-03	9.94E-03
Urinary Bladder Wall	2.99E-03	1.11E-02
Uterus	3.14E-03	1.16E-02
Total Body	2.85E-03	1.05E-02
Effective Dose Equivalent	3.30E-03	1.22E-02
Effective Dose	2.99E-03	1.10E-02

Acute Toxicity study

Following dosimetry estimation, we also evaluated the acute toxicity in mice. A total of 30 mice were divided into 5 groups, which were injected with escalating doses ranging from 82 mg/kg to 168 mg/kg. Based on the survival percentage, we calculated the LD_{50} of MeDAS as 141 mg/kg,

which is well in the safety margin, as it is in the 6 orders of magnitude higher than the amount needed for the *in vivo* PET imaging studies.

DISCUSSION

Multiple sclerosis is the most common of the adult CNS demyellnating diseases. Early in the disease it is characterized by episodes of functional relapse and remission. The biological basis of the relapses and remission is currently unclear. Histological studies imply that intervals of remission are a reflection of remyelination although there is no direct evidence to support this hypothesis. Indeed, relatively little is known about the timing and regulation of CNS remyelination and until the last 5 years there was relatively little effort focused on developing therapies targeted at myelin repair. As a result current therapeutic strategies primarily target the immunopathological basis of demyelination and the outcome from this approach has not been particularly successful, as most therapies continue to be directed toward widespread immuno-suppression, and do little to promote long lasting repair. As such, they are of limited value for supporting long-term functional restoration. For long term functional recovery in patients with MS and related acquired demyelinating diseases, more recent efforts have been made to utilize the information generated from pathobiological studies on the development of myelinating oligodendrocyte to identify targets and characterize new therapeutic approaches towards promoting lasting remyelination in the adult CNS.

For drug discovery and development in myelin repair therapy, one major challenge has been assessing and quantifying changes in myelin content *in vivo*. To date, magnetic resonance imaging (MRI) has been the primary tool for diagnosing and monitoring the demyelinating conditions in MS. Unfortunately, any change in signal intensity on a dual echo T2-weighted sequence reflects a change in tissue water content, which is a non-specific measure of the

overall changes in macroscopic tissue injury and ranges from edema and inflammation, to demyelination and axonal loss. As a result, MRI changes do not specifically reflect changes in demyelination and remyelination and it cannot be used to unambiguously identify effective remyelinating therapies. It is thus essential to develop a measure that will effectively correlate clinical outcomes directly with myelin content. For this reason, we propose to detect and quantify myelin changes based on PET. PET imaging is a noninvasive imaging technique capable of direct characterization and quantification of biological processes at the molecular level (Phelps, 2000). It has become one of the most important clinical techniques in the diagnosis, prognosis, and monitoring of disease progression. This powerful imaging technique is used in conjunction with trace amounts of positron-emitting radiotracers that are specific for targets of interest.

For *in vivo* detection and quantification of myelin changes, radiotracers must readily enter the brain and specifically bind to myelin sheaths. To date, lack of myelin-specific imaging radiotracers has hampered the application of PET in monitoring demyelination and remyelination. As a result, PET study in MS is limited to the characterization of neuroinflammation using [^{18}F]FDG for glucose metabolism or [^{11}C]PK11195 for peripheral benzodiazepine receptors (PBR) mediated microglia activation (Cuzner, 1997; Wilms et al., 2003; Chen and Guilarte, 2006; Buck et al., 2012). However, such radiotracers are not specific for the characterization of demyelination and remyelination, so they do not provide any correlation of disease progression in MS. Most recently, a F-18 labeled mitochondrial 18kDa translocator protein (TSPO) radioligand termed [^{18}F]DPA-714, has also been developed to image microglial/macrophage activation present in the experimental autoimmune encephalomyelitis (EAE) rat model (Abourbeh et al., 2012). Similar to PBR, TSPO only

identifies neuroinflammation (Winkeler et al.; Banati, 2002; Dolle et al., 2009). Thus, [^{18}F]DPA-714 PET can only be used for imaging inflammation, not myelination.

A new strategy is to develop therapeutic agents that are aimed at stimulating remyelination in damaged neural tissues. To date, the development of such myelin repair therapeutics for MS has been hampered by the lack of imaging approaches that allow for direct detection and quantification of myelin changes in a longitudinal manner. In order to meet this challenge, we developed a series of radiotracers for PET imaging of myelination. To identify the most promising PET imaging markers for downstream clinical studies, we used the following set of quantitative acceptance criteria to guide our evaluation processes: 1) High brain uptake at early time points following i.v. injection. At 5 min post injection, the brain concentration of probe should reach 5% ID/g; 2) Average retention in white matter should be at least 20% higher than that in the adjacent gray matter in the spinal cord; 3) In animal models of MS, radioactivity concentration in demyelinated regions should be significantly lower than that in non-demyelinated regions, based on the same size of regions of interest; 4) Radioactive metabolites in plasma should be hydrophilic, and not permeable across the BBB to avoid diluting the specific uptake signal; 5) Rapid clearance of radiotracer from other organs (e.g, lung, heart, liver, etc) to ensure optimal dosimetry; 6) Minimal probe toxicity with an LD50 ≥10 mg/kg, or 1,000 times higher than the amount to be injected in future human subjects to ensure a wide margin of safety.

Accordingly, [^{11}C]MeDAS exhibits a promising profile of *in vivo* binding properties and toxicity. Biodistribution studies showed that it readily entered the brain at early time points with 6.07 ID/g at 5 min. After entering the brain, [^{11}C]MeDAS was proportionally localized in the white matter vs. gray matter. In the brain, the average retention in the white matter is ca. 40% higher

than in the gray matter (**Figure 3A**). In demyelinated regions, the uptake of [^{11}C]MeDAS was significantly decreased. In the model of focal demyelination introduced by LPC, for example, [^{11}C]MeDAS uptake was 34% lower in the demyelinated regions compared to intact myelinated regions in the spinal cord. Further studies showed that the radioactive metabolites of [^{11}C]MeDAS are hydrophilic and expected not to be permeable across the BBB to interfere with the specific uptake signal. Based on the biodistribution studies, the dosimetry of [^{11}C]MeDAS was estimated, and these data sets were all well fit with single exponential functions. Most organs appear to receive around 0.002-0.005 mGy/MBq. The total exposure resulting from a 10 mCi administration of [^{11}C]MeDAS is far below the FDA-defined limits for yearly cumulative and per study exposures to research participants, and is comparable with other radiotracers widely used in the clinic. Acute toxicity studies also showed that [^{11}C]MeDAS was safe for potential human studies, with a LD_{50} of 141 mg/Kg or 6 order of magnitude higher than the actual dose needed for PET imaging studies in humans.

To demonstrate that [^{11}C]MeDAS has the potential to identify potential CNS remyelinating therapies, we have performed proof-of concept studies that demonstrate the ability of the probe to detect therapy induced remyelination in a longitudinal manner. These data, combined with the characterization of [^{11}C]MeDAS binding in the EAE model suggest that the levels of demyelination and remyelination in spinal cord of animals with EAE are considerably more dynamic in both time and location than had been previously appreciated. By analogy, it may well be that current imaging modalities are missing much of the dynamic nature of adult demyelinating diseases and as such fail to provide clarity on the true nature of the disease and its temporal/spatial fluctuations.

CONCLUSION

The studies described above represent a unique imaging-guided approach to monitor disease and repair processes in demyelinating conditions in the CNS, with the absence of invasive surgeries or biopsies. The major advance in being able to utilize our newly developed myelin-imaging technique to quantify local levels of myelination, will for the first time, allow the development of therapeutics that are directly focused at recovery of lost neural tissue. Because myelin repair is critical for sustained functional recovery, the ability to directly track myelin levels in defined regions of the human CNS will allow us to assess the efficacy of new therapeutics in promoting myelin repair. Thus, the threshold for developing new MS therapeutics will be significantly reduced, and this application holds the promise of allowing new therapeutic development to proceed in a highly accelerated manner. As a consequence, the impact on MS patients will be profound as this novel approach could potentially revolutionize therapeutic development for demyelinating diseases, and hasten their widespread clinical application.

REFERENCES

Abourbeh G, Theze B, Maroy R, Dubois A, Brulon V, Fontyn Y, Dolle F, Tavitian B, Boisgard R (2012) Imaging microglial/macrophage activation in spinal cords of experimental autoimmune encephalomyelitis rats by positron emission tomography using the mitochondrial 18 kDa translocator protein radioligand [(1)(8)F]DPA-714. J Neurosci 32:5728-5736.

Bai L, Lennon DP, Caplan AI, DeChant A, Hecker J, Kranso J, Zaremba A, Miller RH (2012) Hepatocyte growth factor mediates mesenchymal stem cell-induced recovery in multiple sclerosis models. Nat Neurosci 15:862-870.

Banati RB (2002) Visualising microglial activation in vivo. Glia 40:206-217.

Buck D, Forschler A, Lapa C, Schuster T, Vollmar P, Korn T, Nessler S, Stadelmann C, Drzezga A, Buck AK, Wester HJ, Zimmer C, Krause BJ, Hemmer B (2012) 18F-FDG PET detects inflammatory infiltrates in spinal cord experimental autoimmune encephalomyelitis lesions. J Nucl Med 53:1269-1276.

Chen MK, Guilarte TR (2006) Imaging the peripheral benzodiazepine receptor response in central nervous system demyelination and remyelination. Toxicol Sci 91:532-539.

Cuzner ML (1997) Microglia in health and disease. Biochem Soc Trans 25:671-673.

Dolle F, Luus C, Reynolds A, Kassiou M (2009) Radiolabelled molecules for imaging the translocator protein (18 kDa) using positron emission tomography. Curr Med Chem 16:2899-2923.

Kerstetter AE, Padovani-Claudio DA, Bai L, Miller RH (2009) Inhibition of CXCR2 signaling promotes recovery in models of multiple sclerosis. Exp Neurol 220:44-56.

Mi S, Hu B, Hahm K, Luo Y, Kam Hui ES, Yuan Q, Wong WM, Wang L, Su H, Chu TH, Guo J, Zhang W, So KF, Pepinsky B, Shao Z, Graff C, Garber E, Jung V, Wu EX, Wu W (2007)

LINGO-1 antagonist promotes spinal cord remyelination and axonal integrity in MOG-induced experimental autoimmune encephalomyelitis. Nat Med 13:1228-1233.

Phelps ME (2000) Positron emission tomography provides molecular imaging of biological processes. Proc Natl Acad Sci U S A 97:9226-9233.

Stabin MG, Sparks RB, Crowe E (2005) OLINDA/EXM: the second-generation personal computer software for internal dose assessment in nuclear medicine. J Nucl Med 46:1023-1027.

Stankoff B, Wang Y, Bottlaender M, Aigrot MS, Dolle F, Wu C, Feinstein D, Huang GF, Semah F, Mathis CA, Klunk W, Gould RM, Lubetzki C, Zalc B (2006) Imaging of CNS myelin by positron-emission tomography. Proc Natl Acad Sci U S A 103:9304-9309.

Wang C, Wu C, Zhu J, Miller RH, Wang Y (2010a) Design, synthesis, and evaluation of coumarin-based molecular probes for imaging of myelination. J Med Chem 54:2331-2340.

Wang C, Popescu DC, Wu C, Zhu J, Macklin W, Wang Y (2010b) In situ fluorescence imaging of myelination. J Histochem Cytochem 58:611-621.

Wang C, Wu C, Popescu DC, Zhu J, Macklin WB, Miller RH, Wang Y (2011) Longitudinal near-infrared imaging of myelination. J Neurosci 31:2382-2390.

Wang Y, Wu C, Caprariello AV, Somoza E, Zhu W, Wang C, Miller RH (2009) In vivo quantification of myelin changes in the vertebrate nervous system. J Neurosci 29:14663-14669.

Wenk GL, McGann-Gramling K, Hauss-Wegrzyniak B, Ronchetti D, Maucci R, Rosi S, Gasparini L, Ongini E (2004) Attenuation of chronic neuroinflammation by a nitric oxide-releasing derivative of the antioxidant ferulic acid. J Neurochem 89:484-493.

Wilms H, Claasen J, Rohl C, Sievers J, Deuschl G, Lucius R (2003) Involvement of benzodiazepine receptors in neuroinflammatory and neurodegenerative diseases: evidence from activated microglial cells in vitro. Neurobiol Dis 14:417-424.

Winkeler A, Boisgard R, Martin A, Tavitian B Radioisotopic imaging of neuroinflammation. J Nucl Med 51:1-4.

Wu C, Wei J, Tian D, Feng Y, Miller RH, Wang Y (2008) Molecular probes for imaging myelinated white matter in CNS. J Med Chem 51:6682-6688.